Research on Engineering Structures & Materials
www.jresm.org
Research Group

Research Article

Study of structural, morphological, and optical properties of Ag@graphene nanocomposites

Safaa Abed Salih [a], Israa Mudher Hassan [b], S.M. Alduwaib [*,c], M.H. Saeed [d]

Department of Sciences, College of Basic Education, Mustansiriyah University, Baghdad, Iraq

Article Info

Article History:

Received 02 May 2026

Accepted 13 Aug 2026

Keywords:

Nanocomposite;
Graphene;
Silver nanoparticles;
Chemical reduction;
Optical properties

Abstract

In this study, Ag@graphene nanocomposites were synthesized in order to examine their structure and optical behavior. For preparation of nanocomposites, silver nanoparticles (AgNPs) were chemically reduced using sodium borohydride. Then, they were integrated with graphene through ultrasonic-assisted mixing. After synthesis of Ag@graphene nanocomposites, they were structurally assessed using various characterization analyses, consisting of X-ray diffraction spectroscopy (XRD), field emission scanning electron microscopy (FESEM), Fourier transform infrared spectroscopy (FTIR), transmission electron microscopy (TEM), energy-dispersive X-ray spectroscopy (EDXS), and Raman spectroscopy. Moreover, the optical behavior of prepared nanocomposites was investigated with UV-Visible absorption and photoluminescence spectroscopy. The results obtained from characterization analyses confirmed that AgNPs were successfully incorporated within the graphene sheets. In addition, the Ag@graphene nanocomposites revealed UV-Visible absorption peaks with higher intensity as well as higher extinction coefficient compared to their individual components, implying that compositing AgNPs with graphene improved their optical properties. These promising optical characteristics could provide a basis for future investigations into the employment of Ag@graphene nanocomposites for different applications, including photocatalysis and optoelectronic.

1. Introduction

The convergence of nanotechnology and material science has enabled the design and fabrication of advanced nanocomposites with tailored physical, chemical, and electronic properties. Among many types of nanomaterials, noble metal nanoparticles, in particular silver nanoparticles (AgNPs), have received lots of interest because of their special physical and chemical properties, including great electrical conductivity, ability to speed up chemical reactions, and strong surface plasmon resonance (SPR) effects [1-3]. However, AgNPs are inclined to clump together and react with oxygen in the air, which can limit their performance over time, especially in devices using light or are hired for chemical reactions [4].

To overcome the aforementioned limitations, compositing AgNPs with two-dimensional (2D) materials, such as graphene, could be a promising strategy. Graphene is a single layer of carbon atoms arranged in a hexagonal pattern, and it exhibits excellent electrical conductivity, vast surface area, high mechanical strength, and remarkable thermal stability [5-7]. These properties have made graphene an ideal substrate or matrix for anchoring metal nanoparticles, thereby stabilizing their structure, enhancing dispersion, and facilitating efficient charge transfer [8-10]. The integration of AgNPs with graphene results in Ag@graphene nanocomposites that exhibit synergistic effects. These nanocomposites not only bring together the benefits of both materials,

*Corresponding author: salah.aldin@uomustansiriyah.edu.iq
[a]orcid.org/0000-0002-6783-0610; [b]orcid.org/0009-0008-6101-9094; [c]orcid.org/0000-0001-5200-5135; [d]orcid.org/0000-0001-6868-3125
DOI: http://dx.doi.org/10.17515/resm2026-1652ma0502rs

but also show better light absorption, improved separation of electrons and holes, and adjustable electronic properties. Such features are particularly attractive for applications in photocatalysis, sensing, plasmonic devices, and surface-enhanced Raman scattering (SERS) [11-14].

Despite numerous studies on individual AgNPs and graphene materials, the structural evolution, interfacial interactions, and optical behavior of Ag@graphene nanocomposites remain subjects of ongoing investigation [15]. The preparation route plays a crucial role in determining the final performance of the composite. Among different methods available for fabrication of Ag@graphene, using chemical reduction to make AgNPs and then, compositing them with graphene through ultrasonic-assisted mixing is simple and cost-effective. Integrating AgNPs with graphene is usually carried out by means of ultrasonication, which ensures that the nanoparticles are evenly spread out on the graphene sheets, resulting in a nanocomposite that has a smooth surface and is stable [16,17].

To scrutinize Ag@graphene nanocomposites, scientists usually adopt X-ray diffraction (XRD) to see the crystal structure, Fourier-transform infrared spectroscopy (FTIR) and Raman spectroscopy to analyze the chemical bonds, and electron microscopy (FESEM/TEM) to look at their shape and size. These tools give information about the microstructures and confirm successful composite formation [18-20]. On the other hand, UV-Visible absorption and photoluminescence (PL) spectroscopy are essential for probing the optical properties and electronic transitions in nanocomposites [21]. Recent studies have shown that integrating AgNPs with graphene matrix could bring about reduction in the bandgap, which improves the ability to absorb visible light and helps electrons move better at the interface [8, 21]. This phenomenon makes such hybrids promising for next-generation optoelectronic systems and energy conversion devices. Additionally, the way light is absorbed and the light emission properties of Ag@graphene composites can be tuned by manipulating the size and the shape of particles [15,22,23].

In the current work, Ag@graphene nanocomposites are synthesized by means of chemical methods in order to closely look at their structures and optical properties. While numerous studies have reported the synthesis and conventional characterization of Ag@graphene nanocomposites, most of which have primarily emphasized on their applications, for instance antibacterial or sensing, with limited attention devoted to a comprehensive examination of their optical behavior. As a consequence, the aim of this study lies in the integrated investigation of the optical characteristics of the Ag@graphene hybrid nanocomposites through complementary UV-Visible absorption and photoluminescence analyses. The combined interpretation of these techniques provides valuable insights into the optical response of the hybrid structures, thereby extending the current understanding of Ag@graphene nanocomposites beyond conventional structural characterization.

2. Experimental Section

2.1 Materials

Silver nitrate ($AgNO_3$, ≥99%) and sodium borohydride ($NaBH_4$, ≥98%) were purchased from Merck. Graphene powder and sodium dodecyl sulfate (SDS) were obtained from Sigma-Aldrich. All experiments were conducted using deionized water as the primary solvent.

2.2 Synthesis of AgNPs

In order to prepare AgNPs, chemical reduction procedure was employed, where silver nitrate acts as the source of silver ions. Initially, 10 mL of 1 mM silver nitrate solution was added dropwise to 30 mL of 2 mM sodium borohydride solution (20 drops per minute), followed by stirring incessantly. Afterward, the resultant mixture was kept in an ice bath at 4 ± 1°C to maintain the nanoparticles stable. In the next step, the solution was centrifuged at 12000 rpm for 15 minutes and then, filtered. Finally, the separated precipitate was washed several times with deionized water, followed by drying at room temperature for 24 hours.

2.3 Synthesis of Ag@graphene Nanocomposite

Fabrication of Ag@graphene nanocomposites was carried out by ultrasonic-assisted mixing approach. In this step, colloidal AgNPs were prepared by dispersing the synthesized AgNPs (section

2.2) in deionized water, followed by sonicating at 400 W for 10 minutes to obtain a homogeneous suspension. To prepare a graphene nanocolloid, 0.2 g of purchased graphene powder and 0.01 g of sodium dodecyl sulfate (SDS), serving as dispersing agent, were added to 200 mL of deionized water. The resulting mixture was sonicated using a 400 W probe sonicator for 20 minutes to obtain a homogeneous and stable colloidal dispersion. At the end, the silver and graphene nanocolloids were mixed (1:1, v/v%), followed by sonicating for 10 minutes to form Ag@graphene nanocomposite. The resultant precipitate was washed several times with deionized water, followed by drying at 60 °C in a vacuum oven for 24 hours.

3. Results and Discussion

3.1 Characterization Tests

Fig. 1 demonstrates X-ray diffraction patterns of AgNPs, graphene, and Ag@graphene nanocomposite. In order to scrutinize crystal structures of nanoparticles and nanocomposites, XRD spectroscopy is commonly adopted. This analysis is also useful for determining the mean size of the crystallites.

As evidenced by XRD pattern of AgNPs depicted in the 2θ range from 20 to 80 degrees, several diffraction peaks are easily detectable at 38.1, 44.2, 64.4, and 77.4°, which respectively correspond to Miller indexes of (111), (200), (220), and (311). The JCPDS file (No. 04–0783) evidences that the peaks match to the face-centered cubic (fcc) structure of metallic Ag [24-27]. The remaining weak reflections not assigned to fcc structure of AgNPs may originate from trace impurities or residual precursor species. Like Ag, XRD spectroscopy was conducted for graphene. According to Fig. 1, a pronounced broad peak at the 2θ of 26.1° and also a weak peak at 42.8° can be found, which are characteristics of graphene's (002) and (100) crystal planes, respectively [28,29].

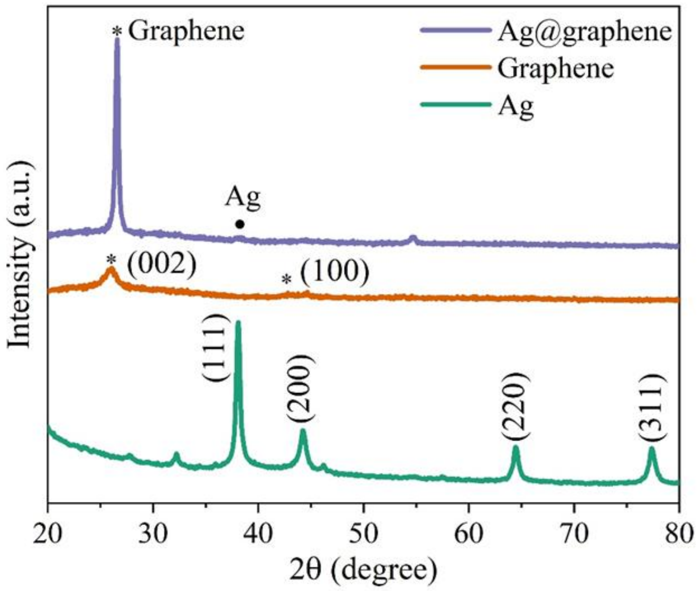

Fig. 1. XRD patterns of AgNPs, graphene, and Ag@graphene nanocomposite

XRD pattern of Ag@graphene nanocomposite can be observed in Fig. 1. In this regard, the characteristic peak related to (002) crystal plane of graphene appears at 26.6°. In addition, the peak showing (111) crystal plane of AgNPs is evident at 38.2°. Consequently, Ag nanoparticles are included within the structure of graphene. The average crystallite size of AgNPs and Ag@graphene could be estimated by Debye–Scherrer's formula, which is as follows [30,31]:

$$D = \frac{K\lambda}{\beta cos\theta} \quad (1)$$

Where D is associated with mean crystallite size, the Scherrer constant (K) equal to 0.98, the X-ray wavelength (λ=1.541 Å), θ exhibits Bragg diffraction angle, and β is imputed to full width at half maximum (FWHM). The FWHM values were obtained through the peak fitting procedure in which Origin software was adopted. Accordingly, the mean crystallite sizes calculated for AgNPs and Ag@graphene respectively are 24 and 34 nm. The results show that incorporation of AgNPs inside graphene resulted in an increment in their size.

Table 1. Peak position and its assigned crystal plane along with FWHM and crystallite size calculated for AgNPs and Ag@graphene

Sample	2θ (°)	Crystal plane	FWHM (°)	Crystallite size (nm)
Ag	38.1	(111)	0.350	24
Ag@graphene	38.2	(111)	0.247	34

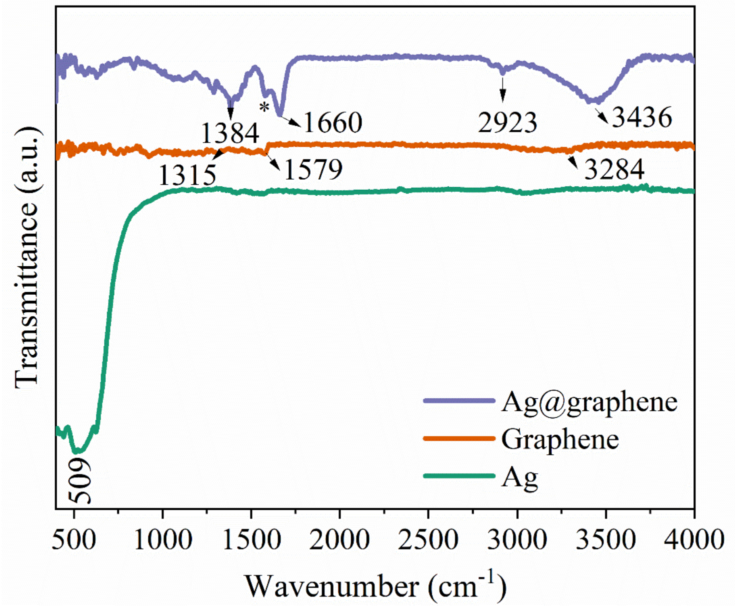

Fig. 2. FTIR spectra of AgNPs, graphene, and Ag@graphene nanocomposite in the wavelength ranging from 400 to 4000 cm^{-1}

FTIR spectroscopy was another analysis adopted for characterization of the fabricated samples. This technique is typically hired to probe the organic and inorganic bonds within the nanoparticles and nanocomposites. Fig. 2 exhibits the FTIR spectrum of AgNPs. In this regard, an absorption band is evident at the wavenumber of 509 cm^{-1}. According to literature, this peak may be associated with interaction of AgNPs with residual surface oxygen-containing species or defect sites present in commercial graphene. Similar interactions between AgNPs and oxygen-containing surface functionalities of graphene-based materials have been reported previously [32].

The FTIR spectrum of graphene is present in Fig. 2. Accordingly, the low-intensity, broad absorption band located at 3284 cm^{-1} is imputed to stretching vibration of hydroxyl (O-H) groups within water molecules [33,34]. In addition, a peak is distinguishable at 1579 cm^{-1}, which is attributed to the stretching mode of the C-C bond [35]. The peak position at 1315 cm^{-1} show stretching vibration of C-O [36].

The absorption bands relevant to Ag and graphene can be seen in the FTIR spectrum of Ag@graphene nanocomposite. In this direction, the peak at 3436 cm^{-1} related to stretching vibration of hydroxyl groups, the peak at 1577 cm^{-1} showing C-C bond (marked by an asterisk), and the peak at 1384 cm^{-1} pertinent to stretching vibration of C-O are observed. Moreover, the peaks features at about 2923 and 1660 cm^{-1} are due to C-H [37] and C=C [38] stretching vibrations, respectively.

Morphological analysis of AgNPs, graphene, and Ag@graphene nanocomposite was carried out by means of FESEM test. According to FESEM image of AgNPs depicted in Fig. 3a, agglomerated spherical-shaped nanoparticles of Ag can be seen. In the FESEM image of graphene Fig. 3b, the layered sheets of this carbonaceous material with full of wrinkles and folded regions can be seen.

Compositing graphene with Ag nanoparticles resulted in its morphology, as evidenced by Fig 3c. Accordingly, and compared to bare graphene Fig. 3b, a much more compact structure can be observed for its counterpart composited with Ag [39]. Moreover, the number of wrinkles and folded regions found for bare graphene decreased in the FESEM image of Ag@graphene composite and a very flat surface is seen for this sample.

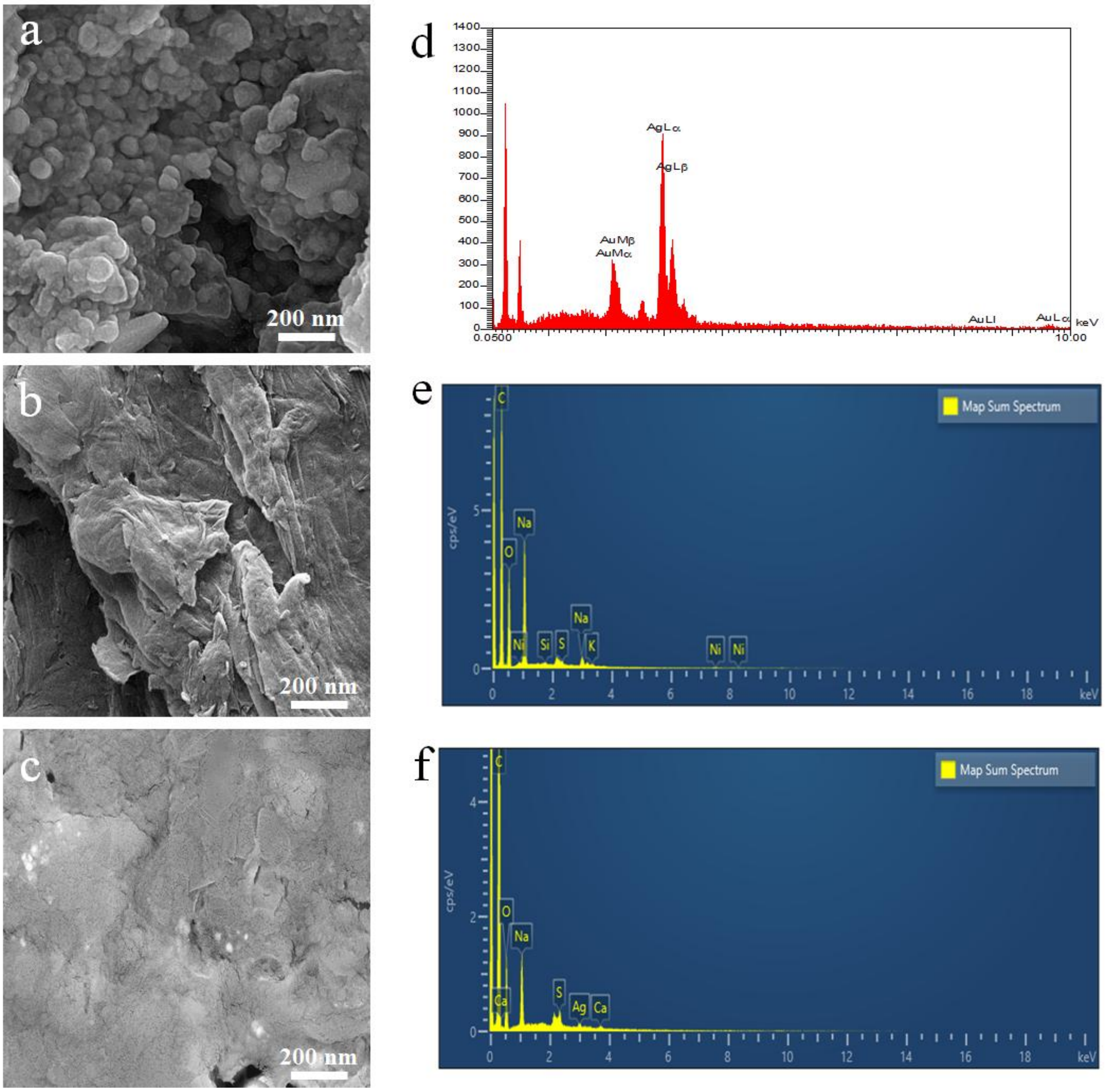

Fig. 3. (a,b,c) FESEM images of AgNPs, graphene, and Ag@graphene nanocomposite, respectively. (d,e,f) EDXS patterns of Ag, graphene, and nanocomposite, respectively

EDXS analysis was utilized to identify elemental composition of prepared samples. In this regard and based on EDXS pattern of synthesized Ag nanoparticles (Fig. 3d), the silver element exhibits a characteristic peak around 3.0 keV. As evidenced by EDXS pattern of graphene (Fig. 3e), the carbon element (C) is detectable peak close to 0.25 keV. Moreover, the oxygen (O) peak element is evident at about 0.5 keV. The oxygen element peak can be arisen from the oxygen-containing bonds like C-O, which were detected by FTIR analysis.

Fig. 3f demonstrates EDXS pattern of Ag@graphene nanocomposite whose quantitative results are tabulated in Table 2. Moreover, the EDXS mapping taken from nanocomposite is available in Fig. 5. Accordingly, the characteristic peak of silver element can be found at 3.0 keV, which attests the presence of Ag nanoparticles in nanocomposite. Carbon and Oxygen give peaks at about 0.25 keV and 0.5 keV, respectively, which were detected in the EDXS pattern of graphene (Fig. 3e). The trace amounts of Au, Na, Si, S, K, Ni, and Ca evident in the EDXS patterns of the samples originate from residual synthesis reagents like SDS, trace impurities within the chemicals, and the Au coating used for FESEM characterization.

Table 2. Quantitative results recorded from EDXS pattern of Ag@graphene nanocomposite

Map Sum Spectrum				
Element	Line Type	Weight %	Weight % Sigma	Atomic %
C	K series	72.62	0.37	79.29
Na	K series	3.30	0.08	1.88
S	K series	0.71	0.05	0.29
Ag	L series	0.75	0.10	0.09
O	K series	22.42	0.37	18.38
Ca	K series	0.20	0.04	0.06
Total		100.00		100.00

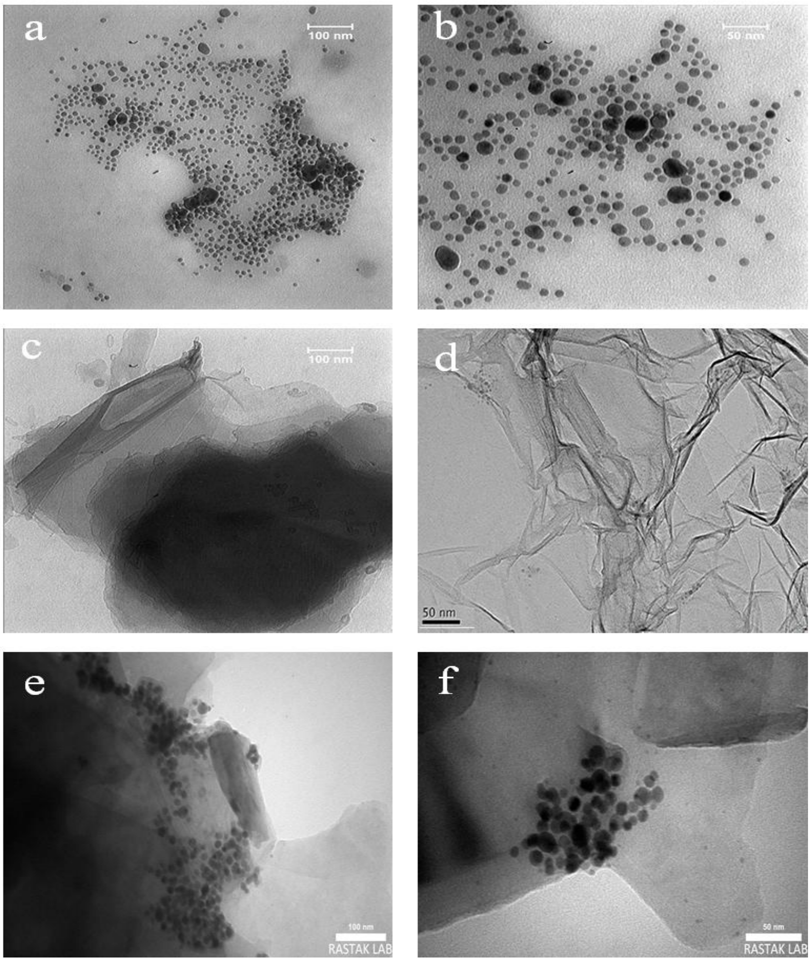

Fig. 4. TEM images of (a,b) AgNPs, (c,d) graphene, and (e,f) Ag@graphene nanocomposite

In addition to FESEM, TEM analysis was used to examine morphology of AgNPs, graphene, and Ag@graphene nanocomposite. (Fig. 4 a, b) illustrates TEM images of AgNPs. Accordingly, the spherical-shaped nanoparticles (size < 25 nm) seen in Fig. 3a can be observed, which are uniformly distributed. In accordance with TEM image of graphene (Fig. 4c), the sheets of graphene are obvious. Lots of wrinkles and folded regions were detected on the surface of graphene sheets (Fig. 3b), which is consistent with its TEM image (Figure 4d). As evidenced by Ag@graphene nanocomposite TEM image (Fig. 4e), the spherical-shaped Ag nanostructures having the size of < 25 nm can be seen, which are evenly dispersed on the surface of graphene sheets (Fig. 5, EDXS mapping of Ag). Compared to bare graphene sheets (Fig. 4d), the ones composited with Ag are much smoother and approximately lack of wrinkles and folded regions (Fig. 4f).

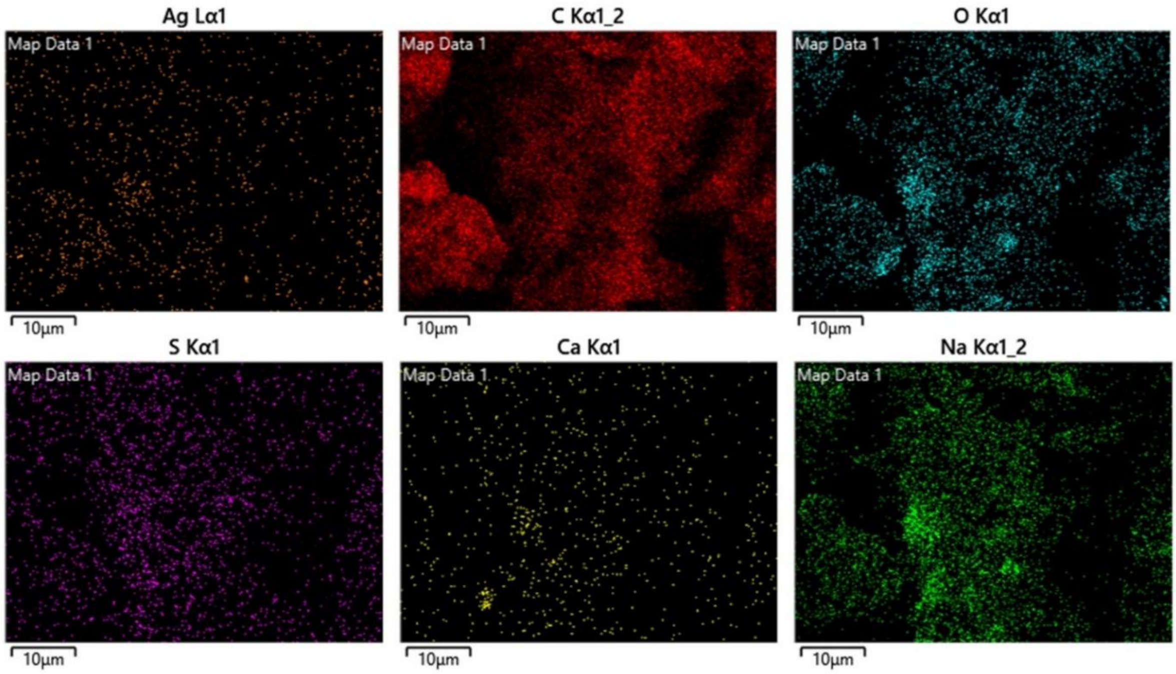

Fig. 5. Elemental mapping taken from the surface of Ag@graphene nanocomposite

Fig. 6 illustrates Raman spectra of AgNPs, graphene, and Ag@graphene nanocomposite, which were recorded using a 532 nm Nd:YAG laser. Fig. 6a demonstrates Raman spectrum of Ag nanostructures. Accordingly, the peaks at 279 and 948 cm^{-1} are reported in some studies on AgNPs [40]; however, their origin remains under debate because metallic Ag does not exhibit conventional first-order Raman modes. Therefore, these bands are regarded only as Ag-related features rather than definitive evidence for metallic Ag. In addition to positions of 279 and 948 cm^{-1}, two well-defined peaks are detectable at ~1580 and near 3000 cm^{-1}.

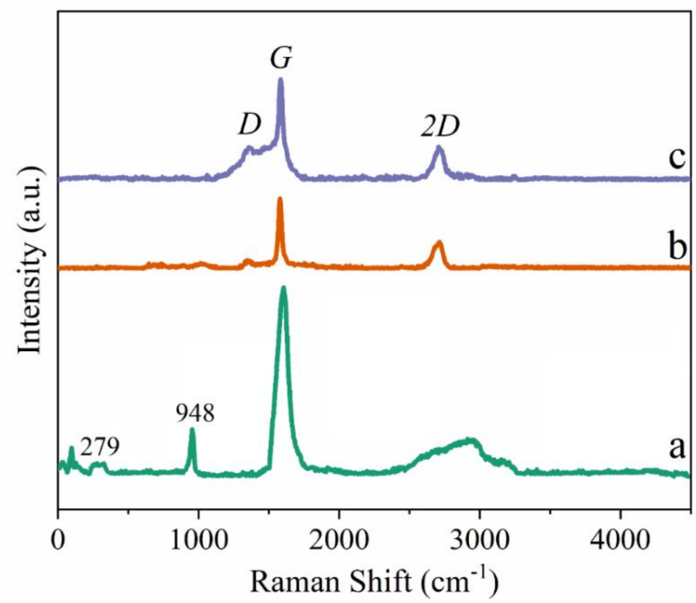

Fig. 6. Raman spectra of (a) AgNPs, (b) graphene, and (c) Ag@graphene nanocomposite

Based on Raman spectra of graphene (Fig. 6b) and its nanocomposite with Ag (Fig. 6c), two noticeable peaks can be observed at 1346 and 1578 cm-1. Referring to literature, in the Raman spectra of carbonaceous materials like graphene two pronounced peaks appear, which are D-band and G-band. The peak situated at 1346 cm^{-1} shows D-band, which is pertinent to sp3 defects in the structure of graphene. D-band could present information regarding surface defects as well as structural imperfections. It has the symmetry of A1g and demonstrates breathing mode of k point phonons [41-44]. Apart from the peak at 1346 cm^{-1}, the peak at 1578 cm^{-1} can also be detected, which is relevant to G-band. G-band has the vibrational mode of E2g and points out in-plane vibration of sp2 carbon atoms. It is an indication for the symmetry and crystallizability of carbon [41-44]. In addition to peaks related to D-band and G band, another peak is evident at 2713 cm^{-1}, which is attributed to 2D band [45]. The peak at ~1580 seen in the Raman spectrum of AgNPs may overlap with G band in spectra of graphene and nanocomposite.

The ID/IG ratio was employed in order to probe structural disorders induced in graphene as a result of compositing process. The higher ratio corresponds to a more disordered structure [42]. In this regard, the ratios calculated for graphene and Ag@graphene are 0.1 and 0.3, respectively, implying an increment in the defect density and structural disorder of the graphene framework after the incorporation of AgNPs.

3.2 Optical Properties Investigation

The optical characteristics of AgNPs, graphene, and Ag@graphene nanocomposite were studied using UV-Visible spectroscopy. As indicated by UV-Visible spectrum of AgNPs (Fig. 7), there are two clear absorption peaks appear, with one near 214 nm and the other around 405 nm. Based on references, the absorption peak of Ag is typically situated at the wavelength of 400 nm [46].

Compared to peak at 405 nm, the one seen at 214 nm is sharper and has more intensity. The UV-Visible absorption spectrum of graphene is illustrated in Fig. 7. Obviously, no definite absorption band is observed for graphene. Compositing AgNPs with graphene gave rise to an increment in the intensity of absorption peaks seen in the spectrum of silver. The UV-Visible absorption spectrum recorded for the Ag@graphene nanocomposite shows similarity to the spectrum recorded for AgNPs. However, the peaks at 214 and 405 nm possess more intensity, which can be ascribed to the efficient role of compositing process.

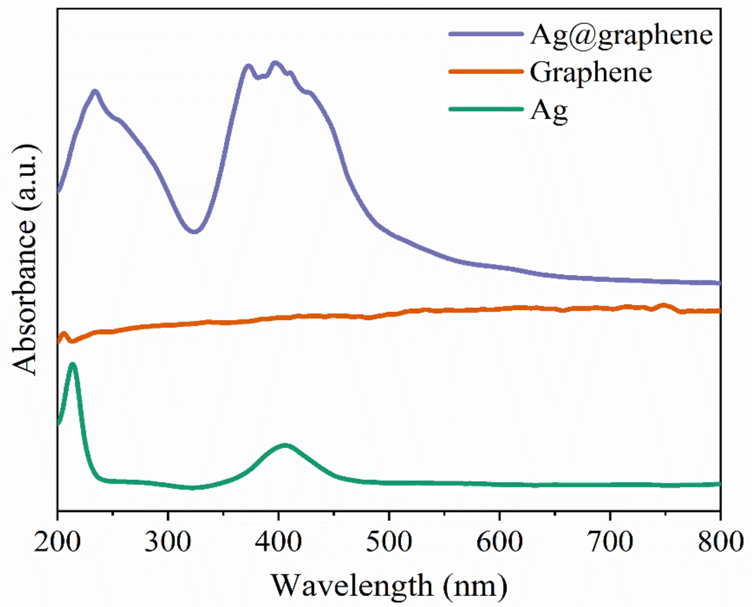

Fig. 7. UV-Visible spectrum of AgNPs, graphene, and Ag@graphene nanocomposite in the wavelength from 200 to 800 nm

In order to obtain energy band gap (Eg) of Ag@graphene nanocomposite, its Tauc's plots was plotted (Fig. 8). For other samples, since Ag is metallic and lacks an intrinsic band gap, and on other hand graphene is a zero-band gap semiconductor or semimetal [47], their Tauc's plots were not drawn for calculation of their Eg values.

The Eg parameter is estimated by extrapolating the straight-line segment of the $(\alpha h\nu)^2$ versus photon energy (hν) curve, which intersects the hν axis. In the Tauc's plot, α is pertinent to the absorption coefficient, h denotes Planck's constant and ν represents the light frequency [48,49]. Accordingly, the band gap value calculated for Ag@graphene is 4.1 eV.

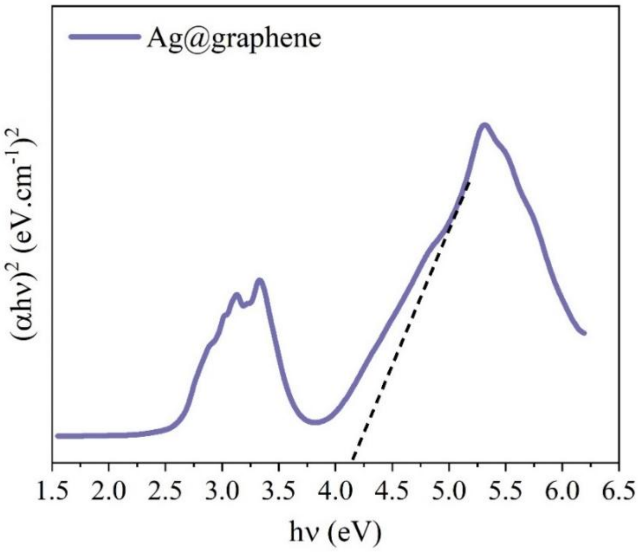

Fig. 8. The Tauc's curve plotted for calculation of band gap energy (Eg) of Ag@graphene nanocomposite

The extinction coefficient curves of AgNPs, graphene, and Ag@graphene nanocomposite are brought in Fig. 9. Extinction coefficient is calculated by the following formula where α and λ respectively are absorption coefficient and wavelength [50,51]. Absorption coefficient is obtained according to the Beer–Lambert law using Equation 3, where A is the measured absorbance and l is the optical path length (l = 1).

$$K = \frac{\alpha\lambda}{4\pi} \quad (2)$$

$$\alpha = \frac{2.303 \times A}{l} \quad (3)$$

Extinction coefficient is a factor for evaluating the ability of a material in absorbing the light. According to Fig. 9, no distinct peak can be seen in the extinction coefficient curve of graphene and it increases linearly by increasing the wavelength. Moreover, the extinction coefficient of Ag@graphene nanocomposite is more than the one obtained for Ag nanostructures, testifying its higher ability in absorbing the light, which is consistent with UV-Visible spectroscopy results.

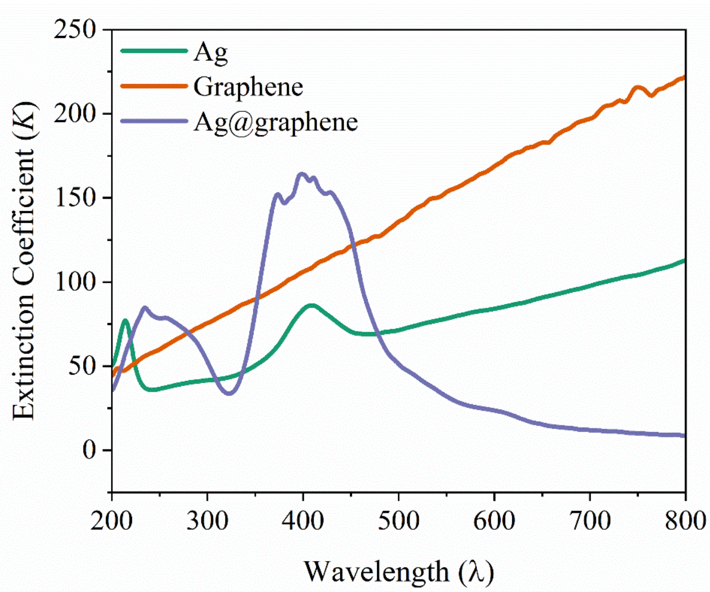

Fig. 9. The extinction coefficient curves of AgNPs, graphene, and Ag@graphene nanocomposite

The Photoluminescence (PL) spectra of AgNPs, graphene, and Ag@graphene nanocomposite are illustrated in Fig. 10. Accordingly, and based on PL spectrum of AgNPs, a distinct emission peak is observed, which is located at 416 nm in the visible spectrum. Referring to literature, the UV emission peaks observed in the PL spectra correspond to near-band-edge emissions, originating from excitonic recombination between conduction band electrons and valence band holes. On the other hand, the emission peaks located in the visible region are deep-level emissions and originated from structural defects for instance oxygen vacancies [52,53]. Like UV-Visible spectrum of graphene, no emission peak is observed in its PL spectrum. However, mixing graphene with AgNPs brought about appearance of a weak broad emission peak, which is in the range from 395 to 435 nm.

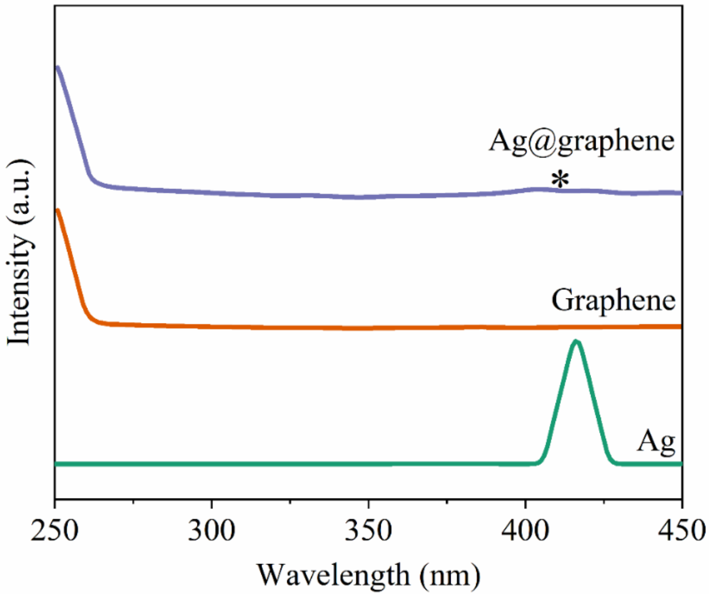

Fig. 10. The PL spectra of AgNPs, graphene, and Ag@graphene nanocomposite

4. Conclusions

In this study, AgNPs, graphene, and Ag@graphene nanocomposite were synthesized to investigate their optical properties, and their structure was analyzed using multiple characterization techniques. As evidenced by XRD technique, AgNPs have face-centered cubic structure. Moreover, the characteristic peak related to (002) crystal plane of graphene was observed in its XRD pattern. The presence of diffraction peaks showing Ag nanostructures and graphene in the XRD pattern of Ag@graphene nanocomposite confirmed its successful fabrication. FTIR was another characterization analysis for structurally investigation of the samples where the main absorption bands of Ag and graphene were detected in the spectrum of nanocomposite. FESEM images revealed that compositing spherical-shaped nanoparticles of Ag with graphene changed the layered structure of graphene into a much more compact one. In addition, compositing decreased the number of wrinkles and folded regions on graphene and made its surface much smoother.

UV-Visible and PL spectroscopy were two analyses employed for evaluation of optical properties of the samples. Unlike graphene showing no absorption peak in its spectrum, two pronounced peaks, mainly the one related to Ag, were observed in the spectra of Ag and nanocomposite. Ag@graphene nanocomposite reached UV-Visible absorption peaks with higher intensity as well as higher extinction coefficient with respect to Ag. The promising optical properties of the Ag@graphene nanocomposite warrant further investigation of its potential in photocatalytic and optoelectronic applications.

References

[1] Rodrigues AS, Batista JGS, Rodrigues MAV, Thipe VC, Minarini LAR, Lopes PS, et al. Advances in silver nanoparticles: a comprehensive review on their potential as antimicrobial agents and their mechanisms of action elucidated by proteomics. Front Microbiol. 2024;15:1440065. https://doi.org/10.3389/fmicb.2024.1440065

[2] Rai MK, Yadav A, Gade A. Silver nanoparticles: the powerful nanoweapon against multidrug-resistant bacteria. J Appl Microbiol. 2012;112(5):841-852. https://doi.org/10.1111/j.1365-2672.2012.05253.x

[3] Prakash J, Ghosh S, Kumar A, Singh M. Synthesis, optical properties and surface enhanced raman scattering applications of noble metal nanoparticles embedded in polymers. Metal Nanoparticles. 2018;125. https://doi.org/10.1007/978-3-319-74814-6_6

[4] Karlo J, Škorić I. Metallic nanoparticles for surface-enhanced Raman scattering based biosensing applications. Photochem. 2024;4(4):417-433. https://doi.org/10.3390/photochem4040026

[5] Novoselov KS, Geim AK, Morozov SV, Jiang D, Zhang Y, Dubonos SV, et al. Electric field effect in atomically thin carbon films. Science. 2004;306(5696):666-669. https://doi.org/10.1126/science.1102896

[6] Geim AK, Novoselov KS. The rise of graphene. Nat Mater. 2007;6(3):183-191. https://doi.org/10.1038/nmat1849

[7] Bonaccorso F, Sun Z, Hasan T, Ferrari AC. Graphene photonics and optoelectronics. Nat Photonics. 2010;4(9):611-622. https://doi.org/10.1038/nphoton.2010.186

[8] Khan M, Tahir MN, Adil SF, Khan HU, Siddiqui MRH, Al-Warthan A, et al. Graphene based metal and metal oxide nanocomposites: synthesis, properties and their applications. J Mater Chem A. 2015;3(37):18753-18808. https://doi.org/10.1039/C5TA02240A

[9] Cheng Y, Zhang H, Zhang Y, Liu J, Li Y. Graphene-supported metal/metal oxide nanohybrids: synthesis and applications in heterogeneous catalysis. Catal Sci Technol. 2015;5(8):3903-3916. https://doi.org/10.1039/C5CY00411J

[10] Khan ZI, Habib U, Mohamad ZB, Tufail A, Raji AM, Khan AU. Innovative hybrid nanocomposites of recycled polyethylene terephthalate/polyamide 11 reinforced with sepiolite and graphene nanoplatelets. J Thermoplast Compos Mater. 2025;38(3):1063-1088. https://doi.org/10.1177/08927057241264457

[11] Rehman R, Zhou Z, Wang H, Imtiaz M. Hybrid materials of graphene and nanoparticles: Synthesis and emerging applications. In: 2D Materials: Chemistry and Applications (Part 1). Bentham Science Publishers; 2024. p. 32-57. https://doi.org/10.2174/9789815223675124010004

[12] Du D, Yang Y, Lin Y. Graphene-based materials for biosensing and bioimaging. MRS Bull. 2012;37(12):1290-1296. https://doi.org/10.1557/mrs.2012.209

[13] Yin PT, Shah S, Chhowalla M, Lee KB. Design, synthesis, and characterization of graphene–nanoparticle hybrid materials for bioapplications. Chem Rev. 2015;115(7):2483-2531. https://doi.org/10.1021/cr500537t

[14] Machado BF, Serp P. Graphene-based materials for catalysis. Catal Sci Technol. 2012;2(1):54-75. https://doi.org/10.1039/C1CY00361E

[15] Lee HK, Lee YH, Zhang Q, Phang IY, Tan HR, Xue C, et al. Designing surface-enhanced Raman scattering (SERS) platforms beyond hotspot engineering: emerging opportunities in analyte manipulations and hybrid materials. Chem Soc Rev. 2019;48(3):731-756. https://doi.org/10.1039/C7CS00786H

[16] Saeed MH, Alduwaib SM, Al-Den DJF. Investigation of structural, photo-luminescence and self-cleaning properties of thin layers of go-zno and go, go-Ag and composite bilayer of go-zno/go-Ag prepared by spray pyrolysis method. Scientia Iranica. 2024;31(12):958-966. https://doi.org/10.24200/sci.2023.60621.6908

[17] Mao M, Hu J, Liu H. Graphene-based materials for flexible electrochemical energy storage. Int J Energy Res. 2015;39(6):727-740. https://doi.org/10.1002/er.3256

[18] Zhang H, Zhang X, Zhang D, Sun X, Lin J, Wang H, et al. Hybridized graphene for supercapacitors: Beyond the limitation of pure graphene. Small. 2021;17(12):2007311. https://doi.org/10.1002/smll.202007311

[19] Eda G, Mattevi C, Yamaguchi H, Kim H, Chhowalla M. Blue photoluminescence from chemically derived graphene oxide. arXiv. 2009. arXiv:0909.2456. https://doi.org/10.48550/arXiv.0909.2456

[20] Ferrari AC, Meyer JC, Scardaci V, Casiraghi C, Lazzeri M, Mauri F, et al. Raman spectrum of graphene and graphene layers. Phys Rev Lett. 2006;97(18):187401. https://doi.org/10.1103/PhysRevLett.97.187401

[21] Alduwaib SM, Salih SA, Fakar Al-Den DJA. Synthesis and characterization of TiO_2-Ag-chitosan nano-composites in order to surface modification and bone tissue engineering using dip coating method. Eng Technol J. 2015;33(5 Pt B):908-922. https://doi.org/10.30684/etj.2015.116698

[22] Zhu Y, Murali S, Cai W, Li X, Suk JW, Potts JR, et al. Graphene and graphene oxide: synthesis, properties, and applications. Adv Mater. 2010;22(35):3906-3924. https://doi.org/10.1002/adma.201001082

[23] Yusaf T, Majeed K, Khan A, Hassan M, Mujtaba MA, Ali HM, et al. A comprehensive review on graphene nanoparticles: Preparation, properties, and applications. Sustainability. 2022;14(19):12336. https://doi.org/10.3390/su141912336

[24] Kalaivani R, Kaviya S, Rajesh S, Bhavani K, Sumedha NC, Karthik S. Synthesis of chitosan mediated silver nanoparticles (Ag NPs) for potential antimicrobial applications. Front Lab Med. 2018;2(1):30-35. https://doi.org/10.1016/j.flm.2018.04.002

[25] Thangamani N, Bhuvaneshwari N. Synthesis, characterization of Ag nanoparticles using the green approach towards degradation of environmental pollutant. J Mater Sci Mater Electron. 2022;33(12):9155-9162. https://doi.org/10.1007/s10854-021-07188-4

[26] Sarkar S, Das R. Shape effect on the elastic properties of Ag nanocrystals. Micro Nano Lett. 2018;13(3):312-315. https://doi.org/10.1049/mnl.2017.0349

[27] Lee JW, Lee J, Kim S, Kim J, Lee S, Park J. Synthesis of silver nanoparticles embedded with single-walled carbon nanotubes for printable elastic electrodes and sensors with high stability. Sci Rep. 2021;11(1):5140. https://doi.org/10.1038/s41598-021-84386-4

[28] Siburian R, Sihotang H, Lumban Raja S, Supeno M, Simanjuntak C. New route to synthesize of graphene nano sheets. Orient J Chem. 2018;34(1):182-187. https://doi.org/10.13005/ojc/340120

[29] Mansoori Mosleh F, Mohammadi A, Hemmati-Sarapardeh A, Schaffie M, Ranjbar M. Asphaltene adsorption onto carbonaceous nanostructures. Energy Fuels. 2020;34(1):211-224. https://doi.org/10.1021/acs.energyfuels.9b03466

[30] Alduwaib SM, Abd MM, Jalaukhan AHA. The structural, optical, and self-cleaning properties of Mn_3O_4/SnO_2 multilayer thin films deposited using spray pyrolysis technique. Scientia Iranica. 2021;28(6):3776-3785. https://doi.org/10.24200/sci.2021.56298.4650

[31] Jadhav GL, Patil DR, Shinde SS, Patil PS. Effect of magnesium substitution on the structural, morphological, optical and wettability properties of cobalt ferrite thin films. Physica B Condens Matter. 2019;555:61-68. https://doi.org/10.1016/j.physb.2018.11.052

[32] Spilarewicz-Stanek K, Kisielewska A, Ginter J, Bałuszyńska K, Piwoński I. Elucidation of the function of oxygen moieties on graphene oxide and reduced graphene oxide in the nucleation and growth of silver nanoparticles. RSC Adv. 2016;6(65):60056-60067. https://doi.org/10.1039/C6RA10483E

[33] Malik SB, Gul A, Saggu JI, Abbasi BA, Azad B, Iqbal J, et al. Fabrication and characterization of Ag-graphene nanocomposites and investigation of their cytotoxic, antifungal and photocatalytic potential. Molecules. 2023;28(10):4139. https://doi.org/10.3390/molecules28104139

[34] Liu Y, Wang L, Wen D, Deng Z, Wu Z, Li S, et al. Preparation and characterization of nano-silver/graphene oxide antibacterial skin dressing. Sci Rep. 2025;15(1):12490. https://doi.org/10.1038/s41598-025-93310-z

[35] Gao R, Hu N, Yang Z, Zhu Q, Chai J, Su Y, et al. Paper-like graphene-Ag composite films with enhanced mechanical and electrical properties. Nanoscale Res Lett. 2013;8(1):32. https://doi.org/10.1186/1556-276X-8-32

[36] Yang Y, Ping Y, Gong Y, Wang Z, Fu Q, Pan C. Ag/graphene composite based on high-quality graphene with high electrical and mechanical properties. Prog Nat Sci Mater Int. 2019;29(4):384-389. https://doi.org/10.1016/j.pnsc.2019.04.010

[37] Peter A, Nicula C, Mihaly Cozmuta A, Drazic G, Peñas A, Silvi S, et al. Polylactic Acid-Based Film Modified with Nano-Ag-Graphene-TiO_2: New Film versus Recycled Film. Adv Polym Technol. 2023;2023:9937270. https://doi.org/10.1155/2023/9937270

[38] Ahmad MA, Aslam S, Mustafa F, Arshad U. Synergistic antibacterial activity of surfactant free Ag–GO nanocomposites. Sci Rep. 2021;11(1):196. https://doi.org/10.1038/s41598-020-80013-w

[39] Habib U, Mohsin MEA, Khan ZI, Mohamad Z, Othman N, Mousa S, et al. Mechanical, thermal, and flammability properties of eco-friendly nanocomposites from recycled PET/PA-11 blends reinforced with graphene nanoplatelets. Polymers. 2025;17(8):1038. https://doi.org/10.3390/polym17081038

[40] Mabrouk MM, El-Din SMM, El-Sayed HS, El-Shafai SA, Abdel-Tawwab M. Impact of aqueous exposure to silver nanoparticles on growth performance, redox status, non-specific immunity, and histopathological changes of Nile Tilapia, Oreochromis niloticus, challenged with Aeromonas hydrophila. Aquac Rep. 2021;21:100816. https://doi.org/10.1016/j.aqrep.2021.100816

[41] Ikram M, Khan A, Imran M, Haider A, Naz S, Ul-Hamid A, et al. Hydrothermal synthesis of silver decorated reduced graphene oxide (rGO) nanoflakes with effective photocatalytic activity for wastewater treatment. Nanoscale Res Lett. 2020;15(1):94. https://doi.org/10.1186/s11671-020-03323-y

[42] Das P, Deoghare AB, Maity SR. A novel approach to synthesize reduced graphene oxide (RGO) at low thermal conditions. Arab J Sci Eng. 2021;46(6):5467-5475. https://doi.org/10.1007/s13369-020-04956-y

[43] Muniyalakshmi M, Sethuraman K, Silambarasan D. Synthesis and characterization of graphene oxide nanosheets. Mater Today Proc. 2020;21:408-410. https://doi.org/10.1016/j.matpr.2019.06.375

[44] Jarvin M, Rajendran S, Kumar R, Silambarasan D, Vengatesan S, Rajesh K, et al. Enhanced photocatalytic performance of Hausmannite Mn_3O_4-rGO nanocomposite in degrading methylene blue. Mater Lett. 2021;305:130750. https://doi.org/10.1016/j.matlet.2021.130750

[45] Mbambo MC, Khamlich S, Khamliche T, Moodley MK, Kaviyarasu K, Madiba IG, et al. Remarkable thermal conductivity enhancement in Ag-decorated graphene nanocomposites based nanofluid by laser liquid solid interaction in ethylene glycol. Sci Rep. 2020;10(1):10982. https://doi.org/10.1038/s41598-020-67418-3

[46] Fu LM, Chen YC, Chen HH, Lin CY, Chen YT. Process optimization of silver nanoparticle synthesis and its application in mercury detection. Micromachines. 2021;12(9):1123. https://doi.org/10.3390/mi12091123

[47] Nigar S, Zhou Z, Wang H, Imtiaz M. Modulating the electronic and magnetic properties of graphene. RSC Adv. 2017;7(81):51546-51580. https://doi.org/10.1039/C7RA08917A

[48] Alduwaib SM, Abd MM. Synthesis and characterization of tungsten carbide (WC)-based nanocomposites and their optical properties and corrosion behavior. Rev Compos Mater Av. 2025;35(5):947-955. https://doi.org/10.18280/rcma.350514

[49] Mursyalaat V, Nurul H, Yusrini, Wiyanto, Yulianti I. The development of program for calculating the band gap energy of semiconductor material based on UV-Vis spectrum using Delphi 7.0. J Phys Conf Ser. 2023;2498(1):012042. https://doi.org/10.1088/1742-6596/2498/1/012042

[50] Messih MA, Ahmed MA, Soltan A, Mohamed RM. Synthesis and characterization of novel Ag/ZnO nanoparticles for photocatalytic degradation of methylene blue under UV and solar irradiation. J Phys Chem Solids. 2019;135:109086. https://doi.org/10.1016/j.jpcs.2019.109086

[51] Moumen A, El-Hilo M, El Marssi M, Sayagués MJ, El Khakani MA, Lassri H. Synthesis and characterization of CuO thin films grown by chemical spray pyrolysis. Opt Quantum Electron. 2017;49(2):62. https://doi.org/10.1007/s11082-017-0910-1

[52] Gandhi AC, Wu SY. Strong deep-level-emission photoluminescence in NiO nanoparticles. Nanomaterials. 2017;7(8):231. https://doi.org/10.3390/nano7080231

[53] Galdámez-Martinez A, Santana G, Güell F, Martínez-Alanis PR, Dutt A. Photoluminescence of ZnO nanowires: A review. Nanomaterials. 2020;10(5):857. https://doi.org/10.3390/nano10050857